

# Photoacoustic Cross-Correlation High-Frame-Rate and Phase Spectroscopy: Two New Biomedical Imaging Modalities

Bahman Lashkari\*, Sung soo Sean Choi, Edem Dovlo, Andreas Mandelis  
Center for Advanced Diffusion-Wave Technologies (CADIFT), Department of  
Mechanical and Industrial Engineering, University of Toronto, Toronto, M5S 3G8,  
Canada

## ABSTRACT

In this study, we present some examples of waveform engineering applications in frequency-domain photoacoustics (FD-PA). Linear frequency modulation (LFM) has been employed in many different fields such as radar, sonar, ultrasound and photoacoustics to perform temporal encoding of the transmitted signal. Encoding the transmission and matched filtering in receive mode tends to increase the signal-to-noise ratio (SNR) while maintaining the resolution. One example of using LFM for photoacoustic spectroscopy is the capability of simultaneous probing/imaging with multiple wavelengths. Use of mismatched coded waveforms enables encoding the signal sources and, therefore, facilitates simultaneous probing and imaging. This method enables high frame rate functional imaging with reduced motion artifacts. Furthermore, it is shown that the phase of the cross-correlation of the PA signal modulated with a linear chirp can yield the absolute absorption coefficient of the chromophore. This method is not affected by attenuation of the fluence due to the absorption and scattering of the overlayer material. Therefore, the method provides a calibration-free approach for quantitative PA imaging. These are some of the features of PA using linear frequency modulation chirp.

**Keywords:** Photoacoustic spectroscopy, frequency-domain photoacoustics, waveform engineering, phase spectroscopy, mismatched coded excitation, frequency modulation

## 1. INTRODUCTION

The flourishing of modern biomedical photoacoustics (PA) for the most part owed to its spectroscopic capability. PA functional imaging can provide a significant impact in preclinical and clinical medicine by characterizing physiological changes and diagnosing the extent of diseases.<sup>1,2</sup> One of the regular targets of PA spectroscopy (PAS) is blood, where PAS help identify and monitor tumor angiogenesis, tumor blood oxygen saturation, and metabolic rate.<sup>3</sup> Thus, PAS can help differentiate between healthy tissue and tumorous lesions, or benign and malignant tumors. Despite the successful record and achievements of PAS, there are some significant challenges that prevent the generation of an accurate quantitative map of the tissue constituents.<sup>4,5</sup> Different approaches have been pursued to enhance the accuracy of PAS. One method is to extract the absorption coefficient from the risetime of the PA response.<sup>6,7,8</sup> Also, the use of acoustic spectra of PA signal vs wavelength provides a calibration-free approach for blood characterization.<sup>9,10</sup> A very different approach is to perform numerical analysis of the laser light diffusion in the tissue while accounting for absorption and scattering of the surrounding tissue.<sup>11,12</sup> This paper introduces a new approach to resolve these issues.

The frame rate of PA imaging and spectroscopy is another factor that will be addressed in this paper. Fast imaging helps reduce motion artifacts. Fast imaging is also a vital requirement for many image-guided intervention applications. These reasons initiated many attempts to increase the PA imaging frame rate or reduce the delay between multiple wavelength emissions employed for PAS.<sup>13,14</sup> The capability of frequency-domain (FD) PA in detecting tumor angiogenesis has been demonstrated before.<sup>15</sup> Additionally, due to the fine control over the excitation frequency range, FD-PA facilitates the spectral analysis of the signal.<sup>16,17</sup> Using FD-PA provides possibilities for waveform engineering that can be employed to enhance specificity, sensitivity, and efficiency of PAS. A few examples of the use of waveform engineering in FD-PA, and particularly PAS are introduced here.

\*bahman@mie.utoronto.ca; phone 1 416 978-1287; fax 1 416 978-6061; mie.utoronto.ca

## 2. HIGH FRAME RATE PHOTOACOUSTIC SPECTROSCOPY

When using a coded excitation waveform, the maximum SNR will be achieved through matched filtering. Alternatively, a mismatched signal can be designed in a way that its cross-correlation (CC) with the transmitted signal is very low. One example is two linear frequency modulations (LFM) with opposite frequency sweep slopes. Figure 1 shows two such chirps with up and down frequency sweeps. Each of these signals generates a very strong cross-correlation with itself and very weak cross-correlation with the other waveform. This property enables the transmission of two coded waveforms simultaneously, followed by decoding the detected signals independently.

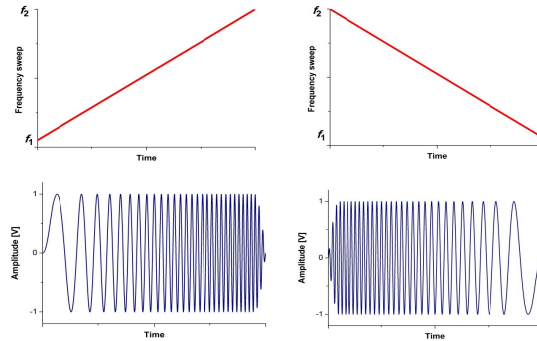


Figure 1. Two linear frequency modulation schemes with up-swept and down-swept frequency chirps.

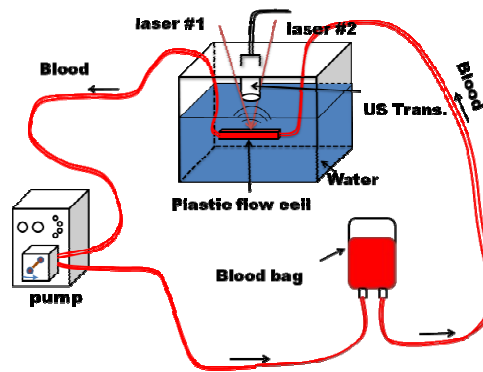


Figure 2. The experimental set-up for PA measurements.

The feasibility of applying mismatched frequency modulation chirps for simultaneous dual-wavelength PAS was demonstrated in an experiment. The oxygen saturation level of circulating sheep blood was probed in two cases of oxygen saturated and deoxygenated blood (Fig. 2). PAS enables the evaluation of blood oxygenation level using two wavelengths, 680 nm and 805 nm in our case. The complete description of experimental set-up is given elsewhere.<sup>18,19</sup> The summary of the instruments involved in the experimental set-up is reported in Table 1.

Table 1. Instrumentation details:

INSTRUMENTATION DETAILS		
Equipment	Manufacturer	Specification
Laser source 1: (LDX Optronics Inc., Maryville, TN, USA)		680 nm
Laser source 2: (Laser Light Solutions, Somerset, NJ, USA)		805 nm
US Transducer 1: V314, (Panametrics, Olympus NDT Inc., MA, USA)		1 MHz
US Transmitter 2: V382, (Panametrics, Olympus NDT Inc., MA, USA)		3.5 MHz
PreAmp 5676 (Panametrics, Olympus NDT Inc., Waltham, MA, USA)		40 dB
Peristaltic pump (Heidolph Instruments GmbH & Co., Germany)		

One experiment was performed on blood exposed to ambient air to become fully oxygen saturated. The experiment was conducted three times, first with 680 nm laser only, then with 805 nm laser only and lastly with both lasers simultaneously. The 680 and 805 nm lasers were modulated with up- and down-swept chirps, respectively (Fig. 1). Figure 3(a)-(c) show the in-phase CC signals generated in the abovementioned three cases. By comparing the CC signals in the dual-waveform case with single laser generated CC cases, it is observed that each waveform operates independently of the other waveform. When one laser is off, its corresponding CC in the figure experimentally demonstrates the correlation of the two mismatched chirps. Figures 3(d)-(f) show a similar experiment on deoxygenated blood. Knowing the intensity of each laser and measuring the peak values, one can obtain the oxygenation level of the blood. Further quantitative results, as well as *in-vivo* simultaneous dual-wavelength PAS using a phased array transducer, have been described elsewhere.<sup>18</sup> It should be added that it is feasible to perform simultaneous imaging with more than two waveforms using mismatched coded excitations.<sup>20</sup> The limitation is the maximum permissible laser exposure.

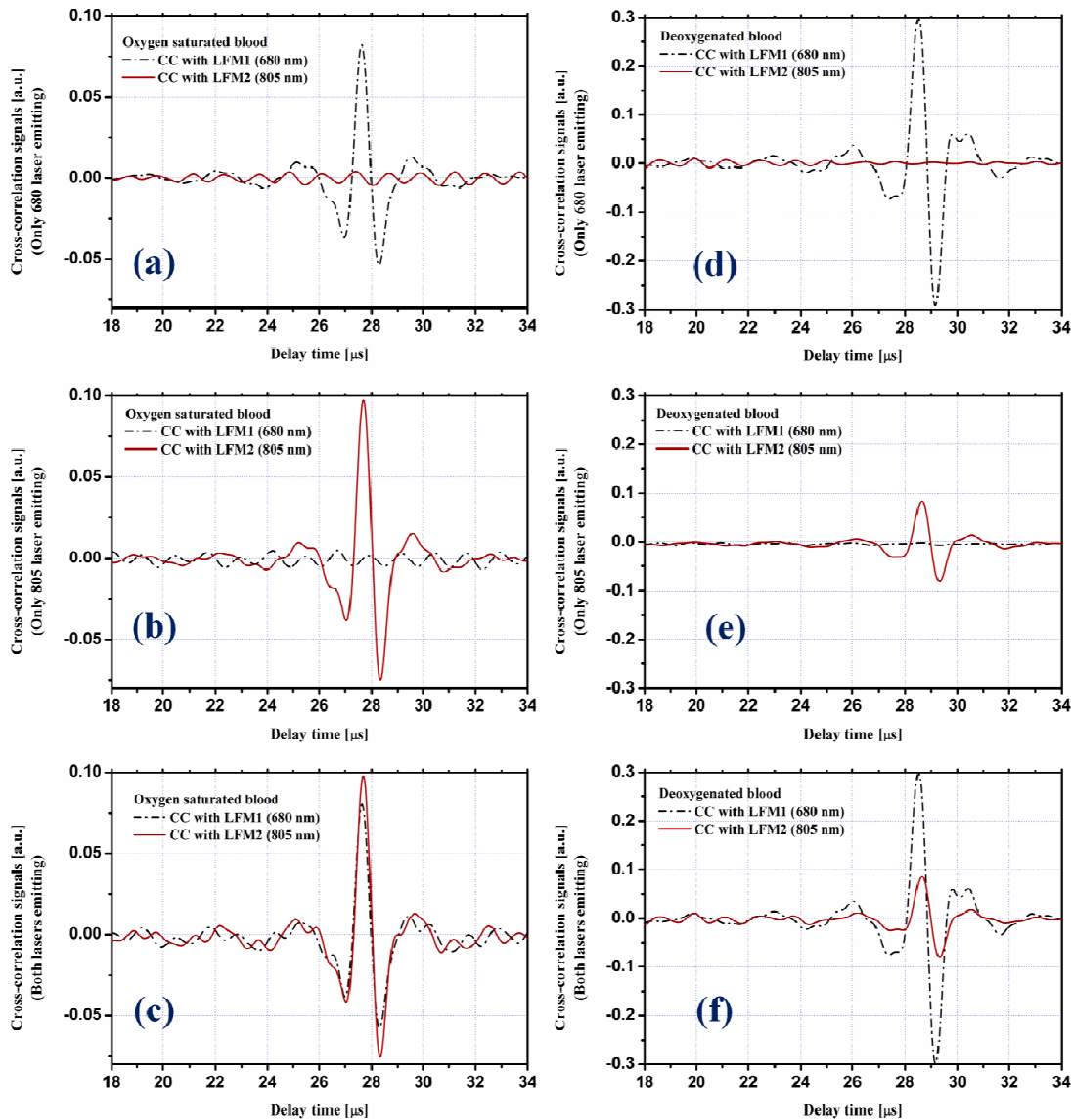


Figure 3. The in-phase cross-correlation signals from oxygen saturated blood with irradiation at (a) 680 nm, (b) 805 nm, and (c) both wavelengths simultaneously. Also shown are the in-phase cross-correlation signals from deoxygenated blood with irradiation of (d) 680 nm, (e) 805 nm, and (f) both wavelengths simultaneously.

### 3. PHOTOACOUSTIC PHASE SPECTROSCOPY

To enhance the sensitivity of frequency-domain PAS, it can be shown that the phase of the PA cross-correlation is affected by the absorption coefficient of the subsurface laser-stimulated chromophores. In the 1D case, the mathematical complexity can be simplified. Therefore, it is both instructive and helpful to demonstrate the analytical relationship. The 1D PA signal generated from a flat semi-infinite absorber is:<sup>21</sup>

$$\tilde{p}_s(-L, f) = \frac{\Gamma e^{-\mu_{eff}L}}{\left(1 + \frac{\rho_a c_a}{\rho_s c_s}\right)} \frac{\mu_a}{\mu_a c_a + j\omega} e^{-jk_s L} \tilde{I}_o(f) \quad (1)$$

where the tilde indicates the Fourier transform operation;  $k_s = \omega/c_s$  is the acoustic angular wavenumber;  $\omega$  is the angular frequency,  $\omega = 2\pi f$ ;  $c_a$  ( $c_s$ ) is the speed of sound in the absorbing (scattering) medium;  $\rho_a$  ( $\rho_s$ ) is the density of the absorbing (scattering) medium;  $\mu_a$  is the absorption coefficient of the absorbing medium;  $\Gamma$  is the Grüneisen parameter;  $\mu_{eff}$  is the effective optical attenuation coefficient of the scattering medium;  $L$  is the thickness of the scattering overlayer medium (the distance of the transducer from the absorber surface);  $I_o$  is the laser intensity on the surface. Applying the 1D theory for linearly modulated laser excitation from frequency  $f_1$  to  $f_2$ , the cross-correlation can be calculated. The bandwidth of the chirp is  $B_{ch} = f_2 - f_1$ . The phase of the cross-correlation signal at distance  $L$  (corresponds to the surface of the chromophore) from the transducer is estimated as:

$$\theta\left(t = \frac{L}{c_s}\right) \approx \tan^{-1} \left\{ \frac{2\pi(f_1 f_2) \ln\left(\frac{f_1}{f_2}\right)}{\mu_a c_a B_{ch}} \right\} \quad (2)$$

Equation (2) shows that the phase of the CC signal is independent of fluence and Grüneisen parameter ( $\Gamma$ ). The phase of the CC signal at delay time  $t = L/c_s$  can readily yield the absorption coefficient of the chromophore:

$$\mu_a \approx \frac{2\pi f_1 f_2 \ln\left(\frac{f_1}{f_2}\right)}{c_a B_{ch} \tan[\theta(t = L/c_s)]} \quad (3)$$

This formula can be used to obtain the absolute absorption coefficient using only one wavelength. A very simple experiment can demonstrate the feasibility of extracting the absorption coefficient of the chromophore from the phase of the PA CC signal. Three PVC-plastisol samples with the approximate absorption coefficients of 4, 6 and 9  $\text{cm}^{-1}$  were produced. The measured in-phase and envelope CC from these samples employing an LFM chirp 300-2.6 MHz is shown in Figs. 4(a) and (b). One of the samples (9  $\text{cm}^{-1}$ ) was employed to calibrate the measurements. The absorption coefficients of the other samples were estimated accordingly as 7.2 and 3.7  $\text{cm}^{-1}$ . The detected signal can be deconvoluted from the effect of the transducer by applying Wiener filtering. One measurement (sample with 9  $\text{cm}^{-1}$  absorption coefficient) was used to obtain the Wiener filter and thus deconvolute the CC signals. From Eq. (3), the absorption coefficients of the other two samples can be obtained through knowledge of the value of  $t = L/c_s$ . To calculate  $t$ , a set of iterative calculations were performed. First, the delay time corresponding to the peak was used to estimate the  $\mu_a$  value. Then, the obtained  $\mu_a$  value was used and the error between the theoretical and experimental signal shape was found, thereby fixing the delay time  $t$  as that which minimizes the error. Through the iterative calculation, best-fitting and correction, the delay time and corresponding  $\mu_a$  were obtained. As a result the estimated values of the absorption coefficients of the two samples were also obtained: 5.8 and 4.1  $\text{cm}^{-1}$ .

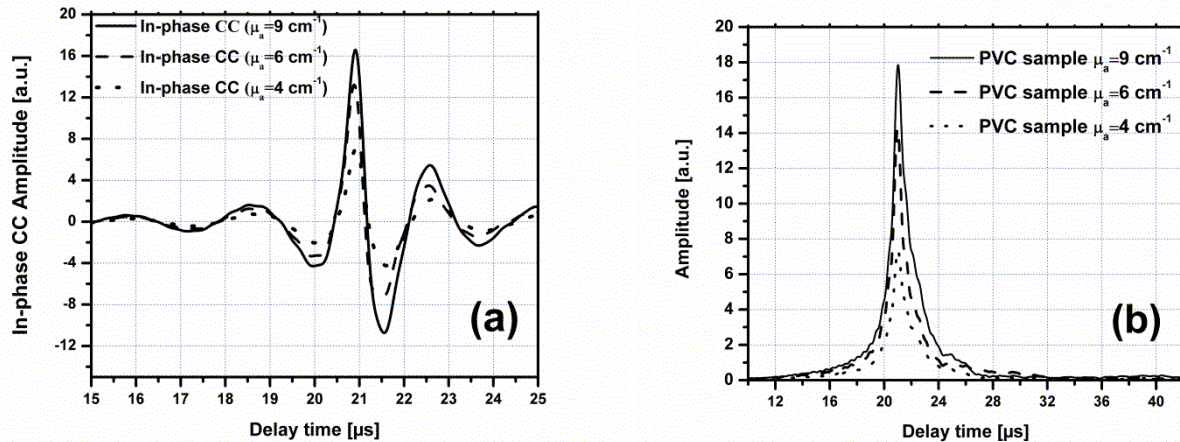


Fig.4 The (a) in-phase and (b) envelope cross-correlation signals from three PVC plastisol samples. (US Trans. 3.5 MHz, Laser light 805 nm, Bandwidth 0.3-2.6 MHz).

As seen from Eq.(3),  $L$  should be known or determined to obtain the  $\mu_a$  values. To simplify the application of the method, one can use an extra wavelength. Using the differences between the absorption coefficients of a chromophore in two wavelengths with no need of absolute values, the tissue can be characterized. Using a Taylor expansion of Eq.(2) for two wavelengths, we obtain:

$$\Delta\theta(t - L / c_s) \approx \frac{B_{ch}c_a}{2\pi f_1 f_2 \ln\left(\frac{f_2}{f_1}\right)} \Delta\mu_a \quad (4)$$

Using well tabulated optical properties of blood, the method can readily be employed for blood spectroscopy. The benefit over using the amplitude values is that the absorption and scattering of the overlaying tissue induces fewer errors. Further experimental results probing *in-vitro* sheep blood are described elsewhere.<sup>22</sup>

#### 4. SUMMARY

In this study, we present some examples of waveform engineering applications in frequency-domain photoacoustics (pa). One example of using linear frequency modulation for photoacoustic spectroscopy is the capability of simultaneous probing/imaging with multiple wavelengths. Use of mismatched coded waveforms enables encoding the signal sources and, therefore, facilitates simultaneous probing and imaging. This method enables high frame rate functional imaging with reduced motion artifacts. Furthermore, it is shown that the phase of the PA cross-correlation induced with a LFM can yield the absolute absorption coefficient of the chromophore. This method is not affected by attenuation of the fluence due to the absorption and scattering of the overlay material.

#### REFERENCES

- [1] Hu, S., and Wang, L.V., "Photoacoustic imaging and characterization of the microvasculature," J. Biomed. Opt. 15(1), 011101 (2010).
- [2] Beard, P., "Biomedical photoacoustic imaging," Interface Focus 1(4), 602-631 (2011).
- [3] Mallidi, S., Luke, G.P., and Emelianov, S., "Photoacoustic imaging in cancer detection, diagnosis, and treatment guidance," Trends in Biotechnology 29(5), 213-221 (2011).

- [4] Cox, B.T., Laufer, J.G., and Beard, P.C., "The challenges for quantitative photoacoustic imaging," *Proc. SPIE* 7177, 13–19 (2009).
- [5] Cox, B., Laufer, J.G., Arridge, S.R., and Beard, P.C., "Quantitative spectroscopic photoacoustic imaging: a review," *J. Biomed. Opt.* 17(6), 061202 (2012).
- [6] Oraevsky, A.A., Jacques, S.L., and Tittel, F.K., "Measurement of tissue optical properties by time-resolved detection of laser-induced transient stress," *Appl. Opt.* 36(1), 402–415 (1997).
- [7] Esenaliev, R.O., Larina, I.V., Larin, K.V., Deyo, D.J., Motamedi, M., and Prough, D.S., "Optoacoustic Technique for Noninvasive Monitoring of Blood Oxygenation: A Feasibility Study," *Appl. Opt.* 41(22), 4722–4731 (2002).
- [8] Petrov, Y.Y., Petrova, I.Y., Patrikeev, I.A., Esenaliev, R.O., and Prough, D.S., "Multiwavelength optoacoustic system for noninvasive monitoring of cerebral venous oxygenation: a pilot clinical test in the internal jugular vein," *Opt. Lett.* 31(12), 1827–1828 (2006).
- [9] Guo, Z., Hu, S., and Wang, L.V., "Calibration-free absolute quantification of optical absorption coefficients using acoustic spectra in 3D photoacoustic microscopy of biological tissue," *Opt. Lett.* 35(12), 2067–2069 (2010).
- [10] Xia, J., Danielli, A., Liu, Y., Wang, L., Maslov, K., and Wang, L.V., "Calibration-free quantification of absolute oxygen saturation based on the dynamics of photoacoustic signals," *Opt. Lett.* 38(15), 2800–2803 (2013).
- [11] Laufer, J., Delpy, D., Elwell, C., and Beard, P., "Quantitative Spatially Resolved Measurement of Tissue Chromophore Concentrations Using Photoacoustic Spectroscopy: Application to the Measurement of Blood Oxygen and Haemoglobin Concentration," *Phys. Med. Biol.* 52, 141–168 (2007).
- [12] Laufer, J., Elwell, C., Delpy, D., and Beard, P., "In vitro Measurement of Absolute Blood Oxygen Saturation Using Pulsed Near-infrared Photoacoustic Spectroscopy: Accuracy and Resolution," *Phys. Med. Biol.* 50, 4409–4428 (2005).
- [13] Yang, J.-M., Favazza, C., Chen, R., Yao, J., Cai, X., Maslov, K., Zhou, Q., Shung, K.K., and Wang, L.V., "Simultaneous functional photoacoustic and ultrasonic endoscopy of internal organs in vivo," *Nat. Med.* 18(8), 1297–1302 (2012).
- [14] Deán-Ben, X.L., Bay, E., and Razansky, D., "Functional optoacoustic imaging of moving objects using microsecond-delay acquisition of multispectral three-dimensional tomographic data," *Sci Rep.* 4, 5878 (2014).
- [15] Dovlo, E., Lashkari, B., Mandelis, A., Shi, W., and Liu, F.-F., "Photoacoustic radar phase-filtered spatial resolution and co-registered ultrasound image enhancement for tumor detection," *Biomed. Opt. Express* 6(3), 1003–1009 (2015).
- [16] Lashkari, B., and Mandelis, A., "Combined photoacoustic and ultrasonic diagnosis of early bone loss and density variations," *Proc. SPIE* 8207, 82076K1–82076K6 (2012).
- [17] Lashkari, B., and Mandelis, A., "Photoacoustic and ultrasonic signatures of early bone density variations," *J. Biomed. Opt.* 19(3), 036015–11 (2014).
- [18] Lashkari, B., Choi, S.S., Khosroshahi, M.E., Dovlo, E., Mandelis, A., "Simultaneous dual-wavelength photoacoustic radar imaging using waveform engineering with mismatched frequency modulated excitation," *Opt. Lett.* 40(7), 1145–1148 (2015).
- [19] Choi, S.S., Mandelis, A., Guo, X., Lashkari, B., Kellnberger, S., and Ntziachristos, V., "Wavelength-modulated differential photoacoustic spectroscopy (WM-DPAS) for noninvasive early cancer detection and tissue hypoxia monitoring," *J. Biophotonics* 1–8, DOI 10.1002/jbio.201500131 (2015).
- [20] Lashkari, B., Zhang, K., Mandelis, A., "High Frame Rate Synthetic Aperture Ultrasound Imaging Using Mismatched Coded Excitation Waveform Engineering. A feasibility study," *IEEE Trans. Ultrason., Ferroelect., Freq. Control* (under review).
- [21] Lashkari, B., and Mandelis, A., "Linear Frequency Modulation Photoacoustic Radar: Optimal Bandwidth for Frequency-domain Imaging of Turbid Media," *J. Acoust. Soc. Am.* 130(3), 1313–1324 (2011).
- [22] Lashkari, B., Choi, S.S., Dovlo, E., Dhody, S., and Mandelis, A., "Frequency-domain photoacoustic phase spectroscopy: A fluence-independent approach for quantitative probing of hemoglobin oxygen saturation," *IEEE J. Sel. Top. Quantum Electron.* 22(3), (DOI 10.1109/JSTQE.2015.2494532) (2016).